Characterization and comparison of iron oxyhydroxide precipitates from biotic and abiotic groundwater treatments

Katarzyna R. Arturi, Christian B. Koch and Erik G. Søgaard

ABSTRACT

Removal of iron is an important step in groundwater treatment for drinking water production. It is performed to prevent organoleptic issues and clogging in water supply systems. Iron can be eliminated with a purely physico-chemical (abiotic) method or biotically with the help of iron-oxidizing bacteria (FeOB). Each of the purification methods requires different operating conditions and results in formation of iron oxyhydroxide (FeOOH) precipitates. Knowledge about the differences in composition and properties of the biotic and abiotic precipitates is desirable from a technical, but also scientific point of view. In this study, a broad spectrum of analytical methods was employed to describe in detail the differences between FeOOH produced in a number of Danish waterworks using either the purely physico-chemical or the biological variation of the iron removal method. According to the results from X-ray diffraction (XRD), small angle X-ray spectroscopy, and visible light microscopy, the precipitate formed with the help of FeOB was more microcrystalline and consisted of agglomerated particles. The purely physico-chemical precipitate was more amorphous and, typically, was composed of smaller particles.

Key words | abiotic iron oxyhydroxides, biotic iron oxyhydroxides, groundwater treatment, iron oxidizing bacteria, iron removal

Katarzyna R. Arturi (corresponding author)
Erik G. Søgaard
Department of Chemistry and Bioscience,
Aalborg University Esbjerg,
Ole Rømers Vej 5,
Esbjerg 6700,
Denmark
E-mail: *kra@bio.aau.dk*

Christian B. Koch
Department of Chemistry,
University of Copenhagen,
Universitetsparken 5,
Copenhagen Ø 2100,
Denmark

INTRODUCTION

The ordinary technique for removal of dissolved iron from groundwater, typically referred to as a purely physico-chemical (or abiotic) treatment, involves aeration of groundwater followed by catalytic oxidation of ferrous iron Fe(II) to ferric iron Fe(III). The simultaneous oxidation and precipitation of ferric oxyhydroxides (FeOOH) take place on the surface of sand grains in in-depth sand filters (Sharma *et al.* 1999, 2001). For groundwaters with high iron concentrations, the purely physico-chemical iron removal is often not sufficient, and Fe can be eliminated biologically (biotically) by the means of iron-oxidizing bacteria (FeOB), a group of morphologically heterogeneous chemolithotrophic procaryotes living in iron-rich environments (Sharma *et al.* 2005; Li *et al.* 2006). Such conditions can be found in many waterworks in Denmark, especially in the southwestern part of Jutland (Søgaard *et al.* 2000, 2001). The biotic and abiotic iron removal techniques are similar in their application in waterworks (aeration followed by filtration), but require different levels of oxygen in the processed raw water to become optimized (10 mg/L and 1 mg/L for the purely physico-chemical and biological iron removal, respectively) (Pacini *et al.* 2014). While high iron and low oxygen contents promote the biologic iron removal and retard its physico-chemical counterpart (van Beek *et al.* 2016), the removal of iron in waterworks employing FeOB is known to be a combination of both processes, resulting

doi: 10.2166/aqua.2017.025

in precipitates of mixed origin. The extent of each process and the final composition of the precipitate depend on the applied process conditions (pH, flow, oxygen content, temperature).

Most of the studies regarding biotic FeOOH precipitates focus on the mechanisms for their formation and the bacterial metabolism (Hallberg & Ferris 2004; Ferris 2005; Bird *et al.* 2011). The mechanisms for the formation of FeOOH in the presence of bacteria are still widely debated. These precipitates may often contain FeOB-originating exopolymers operating as nucleation sites upon which FeOOH precipitate readily. However, it has been proposed that iron precipitation is a secondary effect that could be attributed to the metabolic activity of nitrogen mediating bacteria (Klueglein *et al.* 2014). The composition of the exopolymers has also been disputed widely, and the consensus is that the exopolymers are of organic origin (Chan *et al.* 2009). The general structure of the biotic precipitate has been identified as poorly ordered *ferrihydrite* (Kennedy *et al.* 2003), with few variations (crystalline and amorphous) allowed depending on the conditions (equilibrium and flow, respectively) (Chan *et al.* 2004). Several authors claim that the amorphous *ferrihydrite* of biological origin can crystallize into *goethite* (Kennedy *et al.* 2003) or *lepidocrocite* (Rhoton *et al.* 2002) by aging in water. While the abiotic precipitate has the amorphous structure of *ferrihydrite* (Cornell & Schwertmann 2003), as is expected from a process with high kinetics rates of precipitation, the properties of both precipitates are typically quite different. The biotic precipitate is denser and closely packed, compared to the loosely bound physico-chemical one. The difference is attributed to the cross-bonding of the FeOOH particles by the carbohydrate containing exopolymers (Søgaard *et al.* 2000). Biotic and abiotic iron removal treatments used in drinking water production have been compared many times, mostly concerning the iron removal efficiency (Mouchet 1992; Pacini *et al.* 2005; De Vet *et al.* 2011). According to the results, the presence of FeOB significantly increases the kinetic rates of iron removal (Søgaard *et al.* 2000). From both the scientific and the technical points of view, it would be desirable to discriminate between the biotic and abiotic precipitates, and yet, very few studies have focused on the structure and properties of FeOOH solid by-products from drinking water production. In this study, a broad spectrum of analytical tools was employed to expand the knowledge about the structure and properties of biotic and abiotic FeOOH precipitates. The aim was to describe differences between them in dry conditions and to study the influence of the microbiological activity on the final solid iron containing product. The samples were obtained from several Danish waterworks remediating iron from the groundwater by a purely physico-chemical method or by the means of FeOB. The precipitates were compared with regard to their crystallinity, composition, thermal properties, particle size, morphology, magnetic properties, and fine structure.

MATERIALS AND METHODS

Samples

In this study, precipitates collected at selected Danish waterworks using either the purely physico-chemical or FeOB-based iron removal methods were compared. A high number of waterworks was used in order to cover the natural variation of the precipitates' compositions and to make the results representative (Table 1). While all the samples were studied to obtain the conclusions, only a limited number of distinct and representative results for each group are presented in the figures and tables. The omitted results were almost identical to some of those shown. In order to confirm the type of precipitate, all samples were examined microscopically for the presence of exopolymers shaped as twisted stalks, which are characteristic for *Gallionella ferruginea*. In all samples produced by the purely physico-chemical treatment method, the exopolymers were

Table 1 | Overview of the precipitates' origin

Type	Method	Location	Type	Method	Location
WW	AB	Forum	WW	AB	Jernvedlund
WW	AB	Grindsted (I)	WW	AB	Vester Gjesing
WW	B	Astrup	WW	B	Grindsted (II)
PP	B	Vognsbøl			

WW, waterworks.
PP, pilot plant.
AB, abiotic.
B, biotic.
The Vognsbøl PP has been described in detail by Søgaard *et al.* (2001).

absent. With minor deviations, the waterworks samples were produced according to the previously described groundwater treatment procedure: aeration followed by in-depth sand filtration. The samples were collected from the sand filters during backwashing with air to loosen the precipitate from the sand grains, followed by backwashing with water to remove the precipitate from the filter. The filters at the waterworks typically consist of two layers: (1) fine corned sand (100 cm, grain size 1.0–1.5 mm); and (2) sand grains with increasing diameter for the increasing depth of the filter (1.0–1.4 m, grain size 2–8 mm). The velocity of filtration was ≈5–8 m/h. The velocity of backwash was ≈15–18 m/h. The filter medium at the pilot plant (PP) consisted of sand, 0.5 m deep with a grain size of 1.5 ± 3.0 mm. Sand filters on the PP were cultivated with *G. ferruginea* by mixing new sand grains with the sand grains collected at the Astrup waterworks. The iron content of the groundwater was regulated by addition of $FeSO_4$ (technical grade, JSF, Kemira MiljøA/S). The precipitates were collected as solids dispersed in water by submerging glass bottles during backwashing under the water level of the backwash water, or by using a cup to sample during the aeration part of the backwash process. After the solids had settled, the residue water was removed, and the precipitates were freeze-dried. This method of drying was chosen in order to prevent the disintegration of exopolymers and structural changes to the iron oxyhydroxides.

Crystallinity

A Phillips PW-3064 Spinner X-ray diffraction (XRD, Co-anode; angle range: 10.10–79.90 °2θ; K-α_1, λ: 1.78897 Å; time per step: 6 s/°θ) was used to determine the crystallinity and mineral composition of the sample. The freeze-dried precipitates were homogenized and pressed into a holder. The diffractograms were corrected for the divergence slit intensity, but not the background due to the broad nature of the peaks.

Composition

Elemental composition of the precipitates was determined with a Thermo Electro Corporation atomic absorption spectroscope (AAS). The samples were digested in 7 M HNO_3 (120 °C, 2 bar, 30 min), filtrated through 0.45 μm sterile filters, diluted into range 0–10 mg/L, and analyzed for the major constituents of the precipitates, i.e., for total Fe, Ca, and Mn concentrations. The functional groups present in the samples were identified with a Perkin Elmer PE2000 Fourier transform infrared (FTIR) spectrometer. Infrared spectra were obtained using the KBr pressed pellet technique (≈0.3 mg sample in 300 mg KBr).

Thermal properties

Differential scanning calorimetry (DSC 822 Mettler Toledo) and thermogravimetric analysis (TGA/SDT 851 Mettler Toledo) were used to determine the thermal properties and content of the samples. A dynamic method of heating with a heating ramp of 10 K/min was applied for both DSC and TGA. Measurements were performed in inert and oxidative atmospheres. N_2 was used as a protective gas, while air and O_2 were applied as the reactive gas in the inert and oxidative runs, respectively. The freeze-dried powders were weighted (≈3 mg for DSC and ≈10 mg for TGA), placed in aluminum (DSC) or alumina (TGA) bins, sealed, and analyzed. The TGA analysis was preceded by two blank runs. Each measurement was performed in triplicate.

Particle size and morphology

Small-angle X-ray scattering (SAXS) data were obtained using an adaptation of a Bruker AXS, Nanostar SAXS system, with a rotating anode X-ray generator, cross-coupled Goebel mirrors, three pinholes, and a Bruker AXS Hi-star Area Detector ($Cu - K_\alpha = 1.54$ Å, 0.3×0.3 mm^2 source point, 6 kW power). The scattering intensity (I) was measured, and the data were corrected (background and azimuthal average) to obtain a spectrum of average I vs. q. The results were used to determine the particle size and fractal dimension of the precipitates. The particle size was determined with Guinier approximation for spherical particles ($\ln(I) = \ln(I_0) - \frac{1}{3}R_g^2 \cdot q$). The radius of gyration (R_g) was calculated by extrapolation of intensity at zero scattering angle (I_0) from the $\ln(I)$ vs. q^2 plot. The fractal dimension values were estimated in the Porod's region ($I \approx a + b \cdot q^4$; a,b-constants). Porod's law was extended by changing the

power from 4 to 6-D_F, as the studied FeOOH particles were considered to have complex, and not entirely smooth, surfaces. The values of fractal dimensions (D_F) were extracted from the slope of ln(I) vs. ln(q) plot for high q-values (ln(I) = A-(6-D_F)·ln(q)). The values were determined with SASfit package (version 0.94.0, Joachim Kohlbrecher and Ingo Bressler, Laboratory for Neutron Scattering, Paul Scherrer Institut, Switzerland). The number of points used in calculations was optimized in order to reduce the value of $q \cdot R_g$ (Guinier's region) and to minimize the value of $\chi^2 = \sum_{n=1}^{N} \frac{y_i - CALC_i}{\sigma_i}$ (Porod's region). A Leica visible light microscope with phase contrast and differential interference contrast was used to obtain images of the precipitates recorded with a camera using photo films. A Philips CM20 transmission electron microscope (TEM) was used to view samples air-dried onto copper grids.

Magnetic properties

Magnetic properties of the samples were analyzed with electron paramagnetic resonance (EPR). A Bruker ESP-300E spectrometer operated in the absorption mode at 9.2 GHz, in conjunction with a Varian E-257 variable temperature device and a Hewlett-Packard 5350B frequency counter with a Bruker ER035M NMR gaussmeter were used. The results were recorded as an intensity (I, a.u.) vs. magnetic field (B, Gauss), and converted to I vs. g-values by the formula: $g = (714.484 \cdot \nu)/B$, where ν is frequency (Hz).

Fine structure

Fine structure of the samples was analyzed with Mössbauer spectroscopy. The spectra were obtained using a conventional constant acceleration spectrometer and a ^{57}Co in a Rh source. The spectrometer was calibrated using a 12 μm thick foil at room temperature, and isomer shifts were given relative to the centroid on this absorber. Spectra were measured between room temperature and 5 K using closed cycle and flow-type He cryostats. Hyperfine parameters were obtained by fitting a combination of Lorentzian line-shaped doublet and sextet components constrained to be pairwise identical.

RESULTS AND DISCUSSION

Crystallinity

According to the XRD results, the main constituent of the precipitates, regardless of the applied precipitation method, was amorphous *ferrihydrite*. For the abiotic samples, the amorphous structure was identified as *2-line ferrihydrite*, while the biotic samples resembled the more crystalline *6-line ferrihydrite* (Figure 1). The identified peaks characteristic for *6-line ferrihydrite* included 41.45 °2θ, 46.92 °2θ, 53.80 °2θ, 62.33 °2θ, 72.60 °2θ, and 74.82 °2θ. In both the biotic as well as the abiotic samples, some crystalline minerals were identified, e.g., quartz, chalk, and gypsum. The presence of the first two minerals (or the lack thereof) can be attributed to the composition of the sand filter and the addition of chalk at some of the waterworks. Gypsum was formed by the reaction of sulfate from the groundwater and the chalk. No crystalline forms of iron oxyhydroxides were found in the biotic precipitate. The nature of the registered XRD signal (broad peaks, baseline, high noise level), made it difficult to interpret the data unambiguously and determine the composition with precision. This is not an uncommon phenomenon for XRD analysis of amorphous iron oxides (Carlson & Schwertmann 1981).

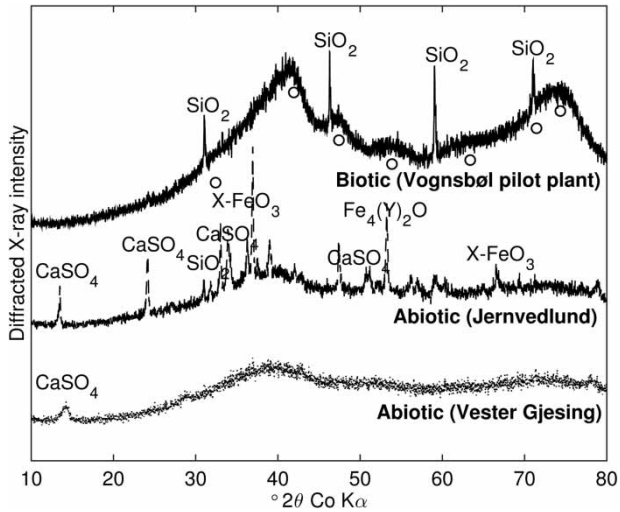

Figure 1 | XRD diffractograms. The characteristic peaks of *6-line ferrihyrdite* are marked with ◦. X and Y represent heterogeneous elements incorporated into the structure of ferrihydrite.

Composition

The composition of the precipitates formed during groundwater treatment depends on the composition of the groundwater, as discussed previously (Czekalla *et al.* 1985). The AAS analysis has shown that the precipitates consisted mainly of FeOOH, minor amounts of calcium, and traces of manganese (Table 2). The abiotic samples were more heterogeneous than the biotic ones, i.e., they contained more calcium. According to the FTIR results (Figure 2), the biotic samples were dominated by many bands indicating the presence of FeOOH: ≈1,000 cm^{-1} (Si-O-Fe and Fe-O-Fe), 538 cm^{-1} and 471 cm^{-1} (Fe-O). Furthermore, the presence of water (-OH stretch) and -COOH groups, which would support the theory about the organic origin of the FeOB stalks, was determined as well (1,633 cm^{-1} and 1,419 cm^{-1}, respectively). In addition to the typical FeOOH absorption bands, the abiotic samples exhibited bands at 1,420, 875, and 712 cm^{-1}, expressing the presence of calcite ($CaCO_3$).

Table 2 | The average content of the precipitates on dry mass basis

Content (wt.%)	Fe	Ca	Mn
Biotic (Waterworks)	43.1	0.4	0.2
Biotic (Vognsbøl PP)	46.9	0.2	0.0
Abiotic (Waterworks)	42.2	2.3	0.2

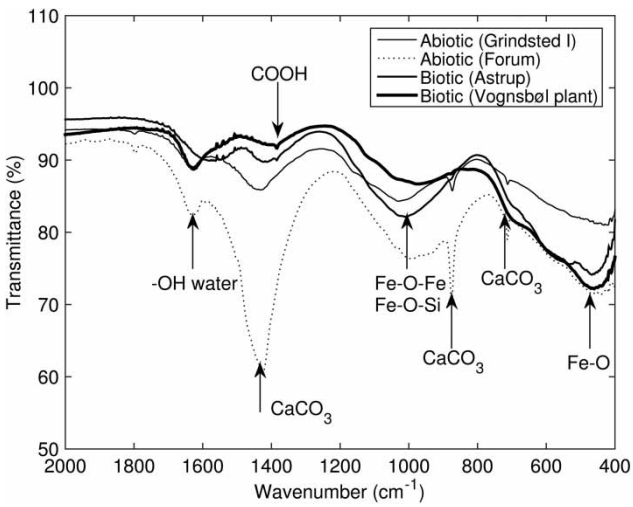

Figure 2 | FTIR results for the range 2,000–400 cm^{-1} showing the bands characteristic for the biotic and abiotic precipitates.

Thermal properties

The obtained DSC and TGA results (Figures 3 and 4, respectively) have shown that the FeOOH precipitates, when heated, undergo both exothermic and endothermic transformations leading to a significant loss of mass (30–35 wt.%), which is in agreement with previous findings (Oliveira *et al.* 2003). For both types of precipitates, the DSC curves were dominated by a broad exothermic peak between

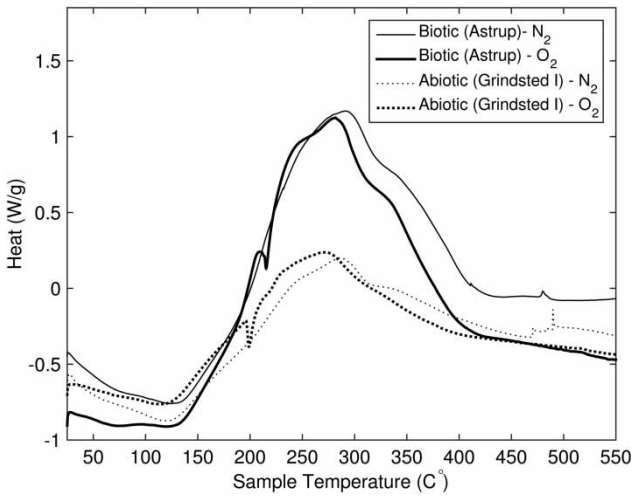

Figure 3 | DSC results showing the exothermic (positive on the Y-axis) and endothermic (negative on the Y-axis) peaks responsible for the thermally induced transformations of the precipitates.

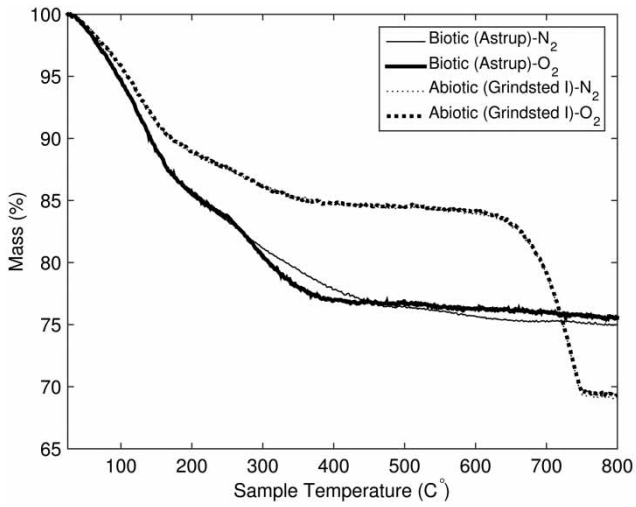

Figure 4 | Mass loss by TGA. The curves for the biotic mass loss, represented with the dashed lines, are completely overlapping.

200 and 400 °C representing the solid–solid transformation of *ferrihydrite* into a more crystalline form of iron oxyhydroxides, e.g., *hematite*. This conversion has begun as an endothermic oxygen uptake at ≈200 °C in the oxygen-rich atmosphere. The process took place through dehydration, dehydroxylation, and rearrangements, and resulted in significant mass loss between 200 and 300 °C for both precipitate types. The biotic *ferrihydrite* was converted more rapidly, as evidenced by higher mass loss gradients and heat values. Above the temperature of 300 °C, the biotic samples continued to lose mass, and the difference between the results procured with O_2 and N_2 could be attributed to the oxidation of the organic core of exopolymers. Above 400 °C, the mass loss for the biotic samples stagnated, while a substantial decrease in the mass, attributed to the decomposition of $CaCO_3$, could be noted for the abiotic samples above 700 °C. The pyrolytic decomposition of the samples in the N_2 atmosphere and oxidation with O_2 resulted in similar final mass losses for the respective types of samples.

Particle size and morphology

According to the SAXS results (Figure 5), the abiotic precipitate consisted of smaller particles, while the biotic precipitation results in the formation of iron hydroxide agglomerates. Although not all requirements for the model were satisfied ($q < 1/R_g$), probably due to the polydispersity and agglomeration of the particles, it was still possible to compute and compare the values for biotic and abiotic precipitates. The average values of the particle size, which were expressed as R_g (Table 3), were larger than previously calculated, most probably due to the unique method of production (Gilbert *et al.* 2009). The D_F values were determined to lie in the range 1–2, lower for the biotic samples than for the abiotic ones, which indicates a lower degree of surface complexity. In general, the computed D_F were quite small. Similar results from laboratory samples were obtained by other authors (Gilbert *et al.* 2007), who explained that the low fractals might be due to the open structure of the clusters. Agglomeration of the particles in the biotic precipitate was seen clearly in the visible light microscopy images presented in Figure 6. The exact structure of the exopolymers observed is shown using TEM (Figure 7).

Magnetic properties

The obtained EPR spectra were shaped as broad tops instead of sharp peaks (Figure 8), which could be attributed

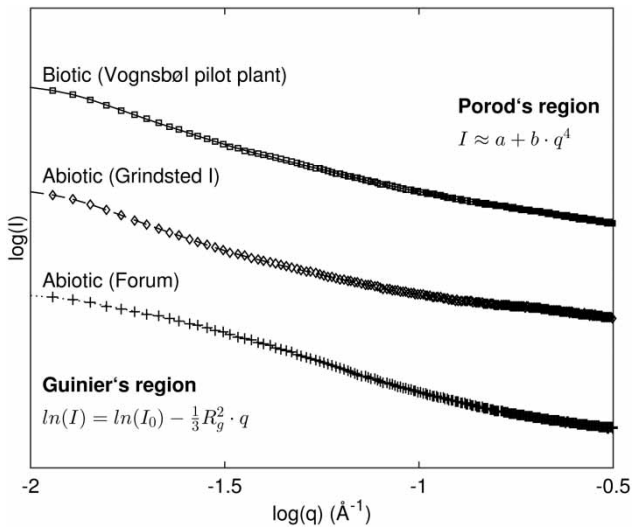

Figure 5 | SAXS results showing the linearity of the curves at the low angles in the Guiniers's region.

Table 3 | The mean particle size and fractal dimension of the biotic and abiotic precipitates calculated from SAXS

Sample	R_g (Å)	D_F
Biotic	152 ± 2	1.47 ± 0.02
Abiotic	115 ± 2	2.02 ± 0.02

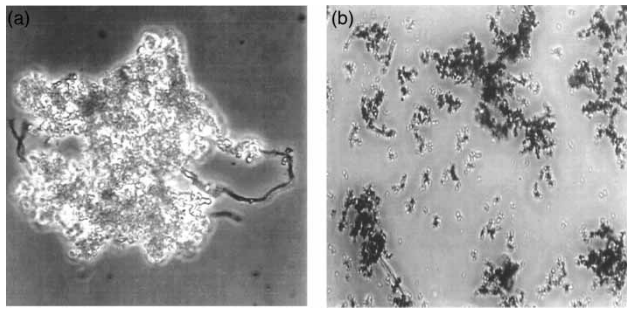

Figure 6 | Light microscopy images (magnification 100×) of the (a) biotic and (b) abiotic iron precipitates.

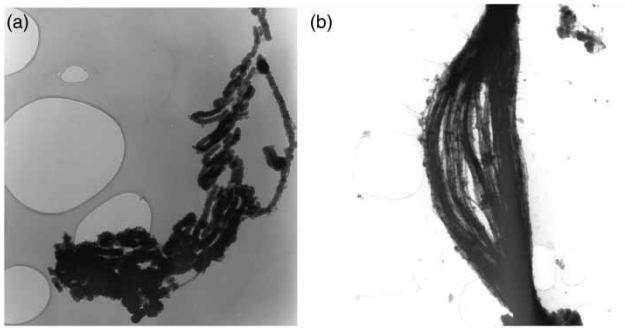

Figure 7 | TEM images of the biotic iron precipitates at magnifications of (a) 20 k and (b) 8.8 k.

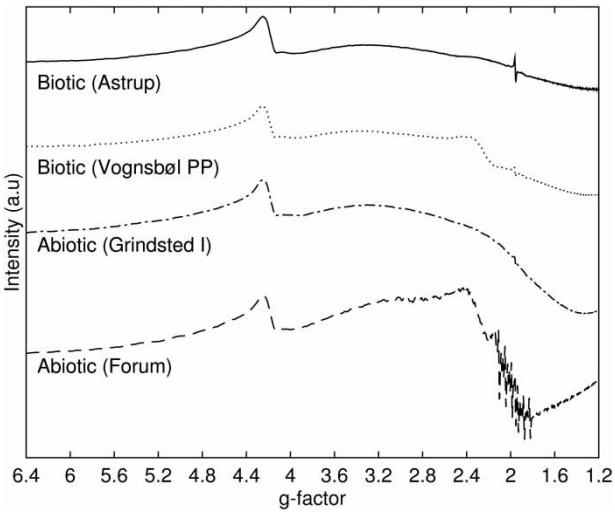

Figure 8 | EPR results showing the 'high-spin' Fe^{3+} split at $g \approx 4.2$ characteristic for FeOOH and a minor hyperfine split sextet pattern characteristic for Mn(II) ($g \approx 2.0$).

to the large amounts of paramagnetic iron in the precipitates. At g-value ≈ 4.2 ($B \approx 1{,}500$ G), a single peak represents 'high-spin' Fe^{3+} in low symmetry (rhombic) and distributed crystal field, as noted previously by Olivié-Lauquet *et al.* (1999). At g-value ≈ 2.0, the presence of manganese is expressed as a sextet pattern characteristic of the hyperfine split $M = -\frac{1}{2} \leftrightarrow +\frac{1}{2}$ central field transition of Mn(II). The minor difference between the EPR spectra of the biotic and purely abiotic samples was related to the exact shapes of the curves. For the biologically precipitated FeOOH samples, the curves were flat, while the precipitates from the purely physico-chemical process resulted in more hill-shaped peaks. This phenomenon could relate to some of the samples' features, most probably the particle size.

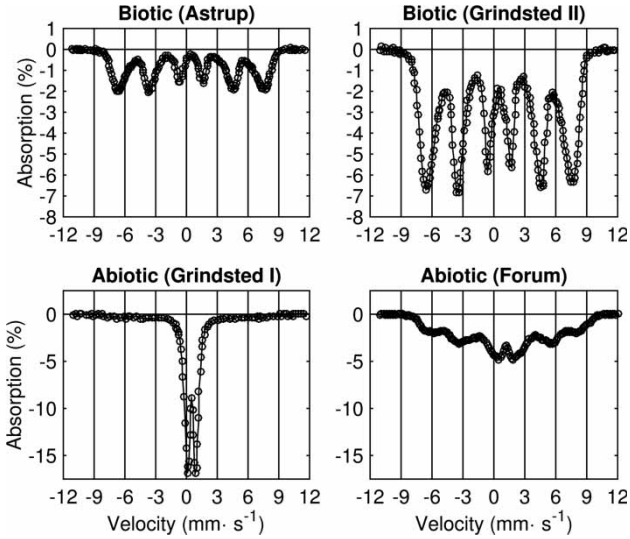

Figure 9 | Mössbauer spectroscopy at T = 15 K showing the major differences between the biotic and abiotic precipitates. At T = 80 K, all samples exhibited the 'one doublet only' behavior typical for the abiotic precipitates, e.g., abiotic Grindsted (I).

Fine structure

Mössbauer analysis has shown that at T = 80 K, all the samples exhibit spectra with one doublet only. The parameters of the doublets ($\Delta E_Q = 0.85 \cdot 0.02\,\mathrm{mm} \cdot s^{-1}$ and $\delta = 0.46 \cdot 0.02\,\mathrm{mm} \cdot s^{-1}$ with a linewidth of approximately $0.50\,\mathrm{mm} \cdot s^{-1}$) were indicative of high-spin Fe(III) with oxygen as a ligand in a relatively distorted octahedra. At T = 15 K, the spectra of the biologically precipitated samples exhibited one sextet with very broad lines (Figure 9). A simple fit of these spectra yielded a magnetic hyperfine splitting of the sextet with a negligible quadruple shift and an outer linewidth $1.66\,\mathrm{mm} \cdot \mathrm{s}^{-1}$. From the temperature scan of the biologically precipitated samples, a blocking temperature of about 35 K was estimated. These parameters are typical for poorly ordered *ferrihydrite*. In contrast, the spectra of the abiotic precipitates contained a doublet component. Here, the samples exhibited behavior either completely dominated by the doublet (≤95%, with similar quadruple splitting at 80 K, and blocking temperature below 15 K), or with partially ordered magnetic spectrum with a magnetic hyperfine field at ≈25 K. Mössbauer spectroscopy has shown that the biotic samples were more easily ordered by lowering the temperature, probably due to the presence of agglomerates. The abiotic

samples were not easily ordered due to the smaller particles. Samples from Grindsted I did not show sign of a sextet even at liquid He temperature (5 K). The iron precipitate collected in Forum contained considerable amounts of manganese, which gave rise to a mixed Mössbauer spectrum.

CONCLUSIONS

A broad spectrum of analytical tools can be used to gain knowledge about the differences between the biotic and abiotic FeOOH precipitates. While the majority of the precipitate consisted of Fe, other elements were present as well, e.g., Ca, Mn, and Si, as evidenced by the applied analytical tools. The structure of the studied iron hydroxides depended primarily on the manner of their formation, i.e., the groundwater treatment technique used. The results have shown that the biotic precipitate is slightly more crystalline than its purely physico-chemical counterpart, yet no purely crystalline iron oxyhydroxides were detected. The difference in the mineral structure was confirmed partly by the thermal analysis, which showed faster -OH desorption and recrystallization of the biotically formed FeOOH. The FTIR indicated the presence of organic -COOH functional groups, which would confirm the organic origin of the exopolymers, and their role as a template for a combined biotic and abiotic iron oxidation and precipitation. The presence of stalks resulted in larger particles forming agglomerates, and thus also a denser precipitate. The differences in particle sizes were also indicated by the EPR and Mössbauer spectral analysis. The biologically precipitated flocs contain carbohydrates and smaller amounts of proteins and fats (Ghiorse 1984). The biotic sludge is much more dense than the purely abiotic physico-chemical precipitate, which appears as distinct colloidal FeOOH particles dispersed in the water. Therefore, the frequency of backwashing the sand filters is lower on waterworks using FeOB than on waterworks using aeration and chemical catalytic precipitation. In the first filtration step, a joint removal of iron, manganese, and arsenic can take place with the help of adsorption and co-precipitation, and that process is improved when a biological iron oxidation/precipitation principle is used at the waterworks. Normally, a second filtration step takes care of manganese removal by increasing pH with the help of strong oxidation of the water from the first filtration step.

ACKNOWLEDGEMENTS

The authors thank Forsyningen, Esbjerg for help with the sampling and Professor Jan Skov Pedersen, Institute of Chemistry and iNANO, Aarhus University, for help with SAXS measurements.

REFERENCES

Bird, L., Bonnefoy, V. & Newman, D. 2011 Bioenergetic challenges of microbial iron metabolisms. *Trends in Microbiology* **19** (7), 330–340.

Carlson, L. & Schwertmann, U. 1981 Natural ferrihydrites in surface deposits from Finland and their association with silica. *Geochimica et Cosmochimica Acta* **45** (3), 421–429.

Chan, C., De Stasio, G., Welch, S., Girasole, M., Frazer, B., Nesterova, M., Fakra, S. & Banfield, J. 2004 Microbial polysaccharides template assembly of nanocrystal fibers. *Science* **303** (5664), 1656.

Chan, C., Fakra, S., Edwards, D., Emerson, D. & Banfield, J. 2009 Iron oxyhydroxide mineralization on microbial extracellular polysaccharides. *Geochimica et Cosmochimica Acta* **73** (13), 3807–3818.

Cornell, R. & Schwertmann, U. 2003 *The Iron Oxides: Structure, Properties, Reactions, Occurrences and Uses.* Wiley-VCH. Verlag GmbH & Co, KGaA, Weinheim, Germany.

Czekalla, C., Mevius, W. & Hanert, H. 1985 Quantitative removal of iron and manganese by microorganisms in rapid sand filters (in situ investigations). *Journal of Water Supply: Research and Technology-Aqua* **3**, 111–123.

De Vet, W., Dinkla, I., Rietveld, L. & van Loosdrecht, M. 2011 Biological iron oxidation by *Gallionella* spp. in drinking water production under fully aerated conditions. *Water Research* **45** (17), 5389–5398.

Ferris, F. 2005 Biogeochemical properties of bacteriogenic iron oxides. *Geomicrobiology Journal* **3** (4), 79–85.

Ghiorse, W. 1984 Biology of iron- and manganese-depositing bacteria. *Annual Reviews in Microbiology* **38** (1), 515–550.

Gilbert, B., Lu, G. & Kim, C. 2007 Stable cluster formation in aqueous suspensions of iron oxyhydroxide nanoparticles. *Journal of Colloid and Interface Science* **313** (1), 152–159.

Gilbert, B., Ono, R. K., Ching, K. & Kim, C. 2009 The effects of nanoparticle aggregation processes on aggregate structure and metal uptake. *Journal of Colloid and Interface Science* **339** (2), 285–295.

Hallberg, R. & Ferris, F. 2004 Biomineralization by *Gallionella*. *Geomicrobiology Journal* **21** (5), 325–330.

Kennedy, C., Scott, S. & Ferris, F. 2003 Characterization of bacteriogenic iron oxide deposits from Axial Volcano, Juan de Fuca Ridge, northeast Pacific Ocean. *Geomicrobiology Journal* **20** (3), 199–214.

Klueglein, N., Zeitvogel, F., Stierhof, Y. D., Floetenmeyer, M., Konhauser, K. O., Kappler, A. & Obst, M. 2014 Potential role of nitrite for abiotic Fe (II) oxidation and cell encrustation during nitrate reduction by denitrifying bacteria. *Applied and Environmental Microbiology* **80** (3), 1051–1061.

Li, D., Zhang, J., Wang, H., Chen, L. & Wang, H. 2006 Application of biological process to treat the groundwater with high concentration of iron and manganese. *Journal of Water Supply: Research and Technology-Aqua* **55** (5), 313–320.

Mouchet, P. 1992 From conventional to biological removal of iron and manganese in France. *Journal of the American Water Works Association* **84** (4), 158–167.

Oliveira, L., Rios, R., Fabris, J., Sapag, K., Garg, V. & Lago, R. 2003 Clay–iron oxide magnetic composites for the adsorption of contaminants in water. *Applied Clay Science* **22** (4), 169–177.

Olivié-Lauquet, G., Allard, T., Benedetti, M. & Muller, J. 1999 Chemical distribution of trivalent iron in riverine material from a tropical ecosystem: a quantitative EPR study. *Water Research* **33** (11), 2726–2734.

Pacini, V. A., María Ingallinella, A. & Sanguinetti, G. 2005 Removal of iron and manganese using biological roughing up flow filtration technology. *Water Research* **39** (18), 4463–4475.

Pacini, V., Ingallinella, A. M., Vidoni, R., Sanguinetti, G. & Fernández, R. 2014 Transformation of an existing physicochemical plant for iron and manganese removal by the application of biological processes. *Journal of Water Supply: Research and Technology-Aqua* **63** (6), 507–517.

Rhoton, F., Bigham, J. & Lindbo, D. 2002 Properties of iron oxides in streams draining the loess uplands of Mississippi. *Applied Geochemistry* **17** (4), 409–419.

Sharma, S., Greetham, M. & Schippers, J. 1999 Adsorption of iron (II) onto filter media. *Journal of Water Supply: Research and Technology-Aqua* **48** (3), 84–91.

Sharma, S. K., Kappelhof, J., Groenendijk, M. & Schippers, J. C. 2001 Comparison of physicochemical iron removal mechanisms in filters. *Journal of Water Supply: Research and Technology-Aqua* **50** (4), 187–198.

Sharma, S. K., Petrusevski, B. & Schippers, J. C. 2005 Biological iron removal from groundwater: a review. *Journal of Water Supply: Research and Technology-Aqua* **54** (4), 239–247.

Søgaard, E., Medenwaldt, R. & Abraham-Peskir, J. 2000 Conditions and rates of biotic and abiotic iron precipitation in selected Danish freshwater plants and microscopic analysis of precipitate morphology. *Water Research* **34** (10), 2675–2682.

Søgaard, E., Aruna, R., Abraham-Peskir, J. & Bender Koch, C. 2001 Conditions for biological precipitation of iron by Gallionella ferruginea in a slightly polluted groundwater. *Applied Geochemistry* **16** (9–10), 1129–1137.

van Beek, C., Dusseldorp, J., Joris, K., Huysman, K., Leijssen, H., Kegel, F. S., de Vet, W., van de Wetering, S. & Hofs, B. 2016 Contributions of homogeneous, heterogeneous and biological iron (II) oxidation in aeration and rapid sand filtration (rsf) in field sites. *Journal of Water Supply: Research and Technology-Aqua* **65** (3), 195–207.

First received 19 April 2016; accepted in revised form 8 November 2016. Available online 19 January 2017